Bulk-surface coupling reconciles Min-protein pattern formation *in vitro* and *in vivo*

Fridtjof Brauns[a,c,1], **Grzegorz Pawlik**[b,1], **Jacob Halatek**[c,1], **Jacob Kerssemakers**[b], **Erwin Frey**[a,2], **and Cees Dekker**[b,2]

[a]Arnold Sommerfeld Center for Theoretical Physics and Center for NanoScience, Department of Physics, Ludwig-Maximilians-Universität München, Theresienstraße 37, D-80333 München, Germany; [b]Department of Bionanoscience, Kavli Institute of Nanoscience Delft, Delft University of Technology, Van der Maasweg 9, 2629 HZ Delft, the Netherlands; [c]Biological Computation Group, Microsoft Research, Cambridge CB1 2FB, UK

Abstract

Self-organisation of Min proteins is responsible for the spatial control of cell division in *Escherichia coli*, and has been studied both *in vivo* and *in vitro*. Intriguingly, the protein patterns observed in these settings differ qualitatively and quantitatively. This puzzling dichotomy has not been resolved to date. Here, we experimentally show that the dynamics crucially depend on the bulk-to-surface ratio, which is vastly different between the cell geometry and traditional *in vitro* setups. We systematically control the bulk-to-surface ratio *in vitro* using laterally wide microchambers with a well-controlled bulk height. A theoretical analysis shows that *in vitro* patterns at low bulk height are driven by the same lateral oscillation mode as pole-to-pole oscillations *in vivo*. At larger bulk height, additional vertical oscillation modes set in, marking the transition to a qualitatively different *in vitro* regime. Our work resolves the Min system's *in vivo*/*in vitro* conundrum and provides important insights on the mechanisms underlying protein patterns in bulk-surface coupled systems.

Min protein patterns determine the mid-cell plane for cell division in many bacteria. They have been intensively studied in *E. coli* where the Min system comprises three proteins: MinC, MinD, and MinE (1–7). These Min proteins alternately accumulate on either pole of the cylindrical cell (8). These oscillations with a one-minute period result in time-averaged Min protein gradients with a minimum concentration at the center of the long cell axis, which localizes the FtsZ-coordinated cell-division machinery to this point (8, 9). The oscillating pattern is driven by cycling of proteins between membrane-bound and cytosolic states, a process governed by cooperative accumulation of MinD (driven by association with ATP) on the membrane and MinD-ATP hydrolysis stimulated by MinE followed by dissociation of both proteins to the cytosol (1, 2, 10). MinC is not involved in the spatiotemporal Min-system dynamics and acts only downstream of membrane-bound MinD to inhibit with the FtsZ polymerization (10–13).

The Min system was discovered *E. coli* (14, 15), and subsequently purified and reconstituted *in vitro* on supported lipid bilayers that mimic the cell membrane (16). This reconstitution provides a minimal system that enables precise control of reaction parameters and geometrical constrains (16–27). This enabled the study of the pattern-formation process and its molecular mechanism in a well-controlled manner, and showed the ability of the Min system to form a rich plethora of dynamic patterns, predominantly travelling waves and spirals, but also "mushrooms", "snakes", "amoebas", "bursts" (16, 17, 28) as well as quasi-static labyrinths, spots, and mesh-like patterns (26, 27). The characteristic length scale (wavelength) of these *in vitro* patterns (with the exception of the quasi-static ones) is on the order of 50 µm — an order of magnitude larger than the approximately 5 to 10 µm wavelength *in vivo* (8, 9). The dichotomy between the disparate Min protein patterns found *in vivo* and those found *in vitro* remained puzzling so far. In particular, it raises the question how these two conditions are related, and, more generally, how we can gain insights on *in vivo* self-organization from *in vitro* studies with reconstituted proteins.

The rich phenomenology of the Min system is remarkable, given its molecular simplicity compared to other pattern-forming systems, such as the Belousov–Zhabotinsky reaction (29–32), or protein-pattern formation in eukaryotic systems (see e.g. (33)). It suggests that a multitude of distinct pattern-forming mechanisms are encoded in the simple Min-protein interaction network. Disentangling and deciphering these mechanisms and the underlying principles poses an ongoing challenge. It is also an opportunity to gain a deeper understanding of fundamental principles underlying pattern formation in general.

Experimental studies of the Min-protein system were closely accompanied by theoretical studies, making the Min-protein system a paradigmatic model system for (protein-based) pattern formation. Modelling and theory have elucidated various aspects of the Min-protein dynamics *in vivo* (34–37) and *in vitro* (16, 23, 26, 38, 39). A particular theoretical insight is that the *same* protein interactions can drive pattern formation through distinct mechanisms in different parameter regimes (26, 37, 39). The most well-known mechanism for protein pattern formation is the so-called "Turing" instability (40) which is a lateral instability that arises due to the interplay of lateral diffusion and local chemical reactions (in our case: protein interactions at the membrane and nucleotide exchange in the bulk). A qualitatively distinct mechanism that can drive pattern formation are coupled local oscillators that form an oscillatory medium (Ref. (41), ch. 4), akin to neurons which can exhibit oscillations individually and yield a rich spatiotemporal phenomenology when coupled, see e.g. (42). The key distinction to the Turing mechanism is that local (nonlinear) oscillators in such systems are able to oscillate autonomously, that is, independently of the lateral coupling to their neighbors (see SI Box 1).

Local oscillations in the *in vitro* reconstituted Min system were theoretically predicted (39), and experimentally observed

F.B., G.P., J.H., E.F., and C.D. designed research; G.P. and C.D. designed and carried out the experiments; F.B., J.H., and E.F. designed the theoretical models and performed the mathematical analyses; F.B., G.P., and J.K. analyzed data; and F.B., G.P., J.H., E.F., and C.D. wrote the paper.

The authors declare no conflict of interest.

[1] F.B., G.P., and J.H. contributed equally to this work.

[2]To whom correspondence should be addressed. E-mail: frey@lmu.de or c.dekker@tudelf.nl

DRAFT

in vesicles (25, 43) where they manifest as homogeneous "pulsing" of the Min-protein density on the vesicle surface. In contrast, in cells such pulsing was never observed, indicating that there are no local oscillation *in vivo*. Instead, the pole-to-pole oscillations in cells are driven by a lateral ("Turing") instability, based solely on the lateral redistribution of proteins (37). The ratio of cytosolic bulk-volume to membrane surface (short: *bulk-surface ratio*) of cells is considerably smaller compared to that of the spatial confinements (vesicles and microchambers) used in reconstitution studies. This suggests that the bulk-surface ratio is the key parameter that distinguishes the *in vivo* regime from the *in vitro* regime — an important hypothesis that merits an in-depth study and experimental verification. Moreover, an analysis of the transition between these two qualitatively different regimes is expected to inform about the organizational principles underlying the system's dynamics.

The key experimental challenge is to systematically control the bulk-surface ratio *in vitro* without influencing the pattern formation process laterally along the membrane. In previous reports, various methods have been employed to enclose the bulk in all three spatial dimensions using microchambers, microwells or vesicles (17, 19, 21, 22, 24, 43). In contrast to the classical *in vitro* setup on a large and planar membrane, patterns cannot evolve freely in such geometries because adaption to the confinement ("geometry sensing") interferes with pattern formation (38, 44, 45). As an illustrative example, consider a traveling wave which is the typical unconfined *in vitro* phenomenon. When a traveling wave is confined to a compartment of size comparable to its wavelength, the wave will be reflected back and forth between the opposite confinement walls and thereby visually resemble a standing wave like the *in vivo* pole-to-pole oscillation, despite the fact that the mechanism underlying these dynamics may be very different (as we will show below). Hence, the *in vivo* and *in vitro* regimes cannot be straightforwardly distinguished in three-dimensionally confined geometries (9, 22).

Here, we eliminate the interfering effects of geometric confinement by using laterally large microchambers with flat surfaces on top and bottom and well-controlled heights between 2 to 60 µm (see Fig. 1A). The microchambers' height of directly controls the bulk-surface ratio, while the MinE patterns on the membranes can evolve freely in lateral directions along the surfaces.

In experiments with reconstituted Min proteins in such microchambers, we observe a rich variety of patterns from standing wave chaos at low bulk heights ($< 8\,\mu m$), to sustained large-scale oscillations at intermediate bulk heights ($\approx 15\,\mu m$), to traveling waves at large bulk heights ($> 20\,\mu m$). The mathematical analysis of the reaction–diffusion equations (homogeneous steady states and their linear stability analysis) in the microchamber geometry with planar, laterally unconfined surfaces enables us to identify the characteristic modes that drive pattern formation. From these modes, we predict a number of signature features of the distinct mechanisms — lateral and local oscillations — underlying pattern formation, in particular the synchronization of patterns between the microchamber's top and bottom surface. We verify these predictions experimentally and thereby provide evidence that indeed distinct lateral and local oscillations underlie pattern formation in the various parameter regimes. Importantly, we find that the patterns in microchambers with low bulk height are driven by the same lateral oscillation mechanism as *in vivo* pole-to-pole oscillations. In contrast, a combination of both lateral and local oscillations govern pattern formation at the large bulk heights that are typical in most traditional *in vitro* setups.

Taken together, we find that the *in vivo* vs *in vitro* dichotomy can be excellently reconciled on the level of the underlying mechanisms. Systematic variation of the bulk height experimentally confirms our theoretical prediction that the bulk-surface ratio is the key parameter that continuously connects the *in vivo* and *in vitro*.

Results

Finite bulk heights lead to drastically different Min patterns. To study the effect of the bulk-surface ratio on Min pattern formation *in vitro*, we need to control this parameter without imposing lateral spatial constraints that affect pattern formation. To achieve this, we created a set of PDMS-based microfluidic chambers of large lateral dimensions ($2\,mm \times 6\,mm$) but with a low height in a range from 2 to 57 µm (Fig. 1*A*). In these wide chambers, patterns can freely evolve in the lateral direction while we study the effects of the bulk-surface ratio which is controlled by the microchamber height. All inner surfaces of the microchambers were covered with supported lipid bilayers composed of DOPG:DOPC (3:7) which has been shown to mimic the natural *E. coli* membrane composition (20). Proteins were administered by rapid injection of a solution containing 1 µM of MinE and and 1 µM of MinD proteins, together with 5 µM ATP and an ATP-regeneration system (22).

Figure 1*C* and Movie S1 show snapshots and kymographs of the characteristic patterns observed in microchambers of different heights. We clearly observe distinct Min patterns that can be identified qualitatively by simple visual inspection: standing wave chaos, "large-scale oscillations", and traveling waves. Next, we will qualitatively describe these different pattern types in detail. Further below in the section *Competition of different oscillation modes leads to multistability of patterns*, we will provide a detailed quantification of the pattern characteristics (wavelength, frequencies, and propagation velocities, based on auto-correlation analysis) in dependence of bulk height and E-D ratio. There we will also show that the different pattern types exist in overlapping regions of the parameter space (bulk height, E-D ratio).

At low bulk height (2–6 µm in Fig. 1*C*) we observe incoherent wave fronts of the protein density propagating from low density towards high density regions, thus continually shifting these regions in a chaotic manner as can be seen in the kymographs. We will refer to these patterns as standing wave chaos. The chaotic character is also evidenced by the irregular shapes and non-uniform propagation velocities of wave fronts within the same pattern (see Fig. S1). Still, these patterns clearly have a characteristic length scale.

At an intermediate bulk height (13 µm in Fig. 1*C*), we observe patterns with large areas that have fairly homogeneous Min-protein density and temporally oscillate as a whole. We refer to these patterns as large-scale oscillations. (We will use this rather general term to subsume a wide range of phenomena that are commonly found in oscillatory media.) Phenomenologically similar oscillations have been observed as

DRAFT

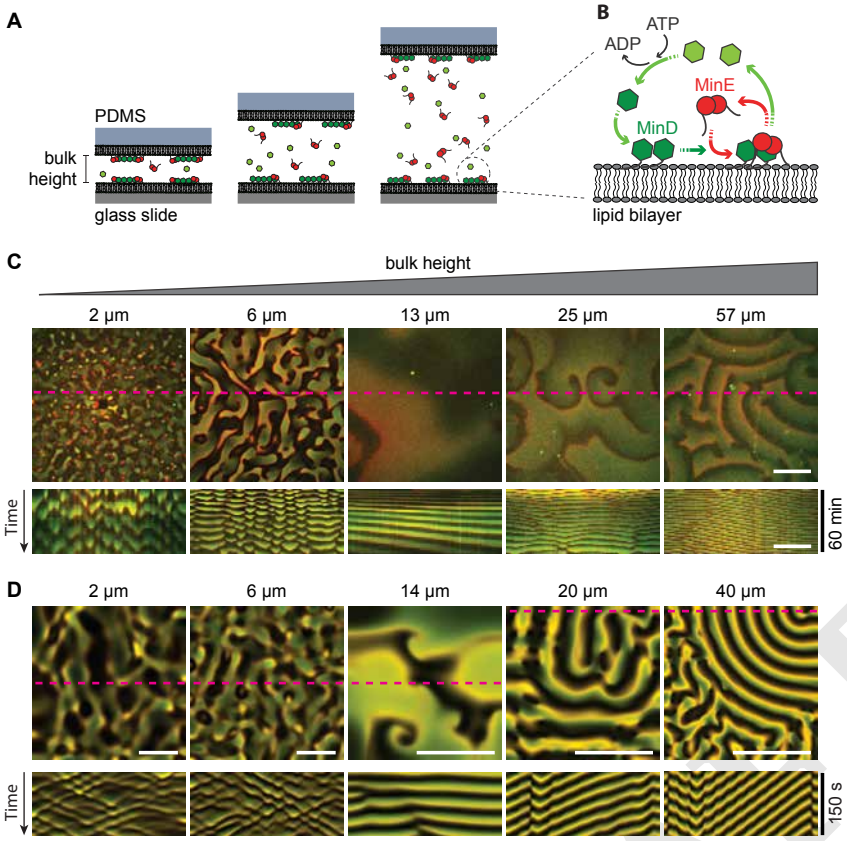

Fig. 1. Effect of a change of a bulk height on Min patter formation. A General concept of the experimental setup. MinD and MinE proteins were reconstituted in laterally large and flat microchambers of different heights. All inner walls of microchambers were covered with supported lipid bilayers made of DOPC:DOPG:TFCL (66 : 32.99 : 0.01 mol%) mimicking the *E. coli* membrane composition. Min proteins cycle between bulk and the membrane upon which they self-organize into dynamic spatial protein-density patterns. **B** Min-protein interaction scheme. MinD monomers (light-green hexagons) bind ATP resulting in dimerization and cooperative accumulation on membrane (dark-green hexagons). Next, MinE dimers bind to MinD, activating its ATPase activity, detachment from the membrane, and diffusion to the bulk where ADP is exchanged to ATP, and the cycle repeats. **C** Influence of the bulk height on Min pattern formation. Snapshots show overlays of MinD channel (green) and MinE channel (red) 30 minutes after injection. Kymographs below were generated along the dashed red lines. In each microchamber, the concentrations of the reconstituted proteins are 1 µM MinE and 1 µM MinD (corresponding to a 1:1 E-D ratio). (White scale bar: 50 µm.) **D** Snapshots and kymographs from numerical simulations of the reaction–diffusion model describing the skeleton Min-model in a three-dimensional box geometry with a membrane on top and bottom surfaces and reflective boundaries on the sides (see SI Materials and Methods for details). The colors are an overlay of MinD density (green) and MinE density (red) on the top membrane. Parameters (from left to right): H = 2 µm, E/D = 0.8; H = 6 µm, E/D = 0.75; H = 14 µm, E/D = 0.75; H = 20 µm, E/D = 0.725; H = 40 µm, E/D = 0.625. The remaining, fixed model-parameters are given in the SI Materials and Methods (Table S1).

an initial transients in some previous experiments (17, 46). In contrast, however, the oscillations that we observed at intermediate bulk heights persisted throughout the entire duration of the experiment (90 minutes).

The lack of spatial coherence for large-scale oscillations is in stark contrast to the traveling waves we observed in the large height regime (57 µm in Fig. 1*C*). Traveling waves are characterized by high spatial coherence of the consecutive wave fronts that propagate together at the same velocity and with a well-controlled wavelength. Finally, the wave patterns found at 25 µm shows phenomena indicative of defect-mediated turbulence: continual creation, annihilation, and movement of spiral defects (Movie S2). This behavior is commonly found in oscillatory media at the transition between spiral waves and homogeneous oscillations / phase waves (47, 48).

Taken together, we find that the bulk height has a profound effect on the phenomenology of Min protein pattern formation. Notably, the bulk-surface ratio at the lowest bulk height (2 µm) is of the same order of magnitude as in *E. coli* cells which have a diameter of about 0.5–1 µm. However, there is no obvious phenomenological correspondence between the *in vivo* system and the laterally unconfined *in vitro* system as the patterns found in these two settings differ qualitatively. Moreover, at low bulk heights, where the bulk-surface ratio is on the same order of magnitude as *in vivo*, the pattern wavelength *in vitro* is approximately 40 µm (see *Quantification of experimentally observed patterns*). This is much larger than the typical wavelength *in vivo* (approximately 5 to 10 µm), as found for stripe oscillations in filamentous cells (8) and large "sculpted" cells (9). We will further elaborate on the question of pattern wavelength in the discussion section.

A minimal model reproduces the salient, qualitative pattern features. To explain the observed diversity of patterns found in experiments, we performed numerical simulations and a theoretical analysis. We used a minimal model of the Min-protein dynamics that is based on the known biochemical interactions between MinD and MinE (Fig. 1*B*). This model encapsulates the core features of the Min system and has successfully reproduced and predicted experimental findings both *in vivo* (36–38) and *in vitro* (23, 39). Finite-element simulations of this model in the same geometry as the microchambers (laterally wide cuboid with membrane on both top and bottom surfaces, see Fig. S2) qualitatively reproduce the three pattern types found in experiments the three regimes of bulk heights, as shown in Fig. 1*D* and Movie S3.

At low bulk heights (0.5–5 µm), the model exhibits standing wave chaos (incoherent fronts that chaotically shift high- and low-density regions) in close qualitative resemblance of the patterns found experimentally. At intermediate bulk heights (5–15 µm), we find nearly homogeneous oscillations, meaning large areas with a nearly homogeneous oscillator density that are phase separated by phase defect lines where the oscillator phase jumps. Shallow gradients in the oscillation phase lead to the impression of propagating fronts, with a velocity inversely proportional to the phase gradient (sometimes called "pseudo waves" or "phase waves" in the theoretical literature (49, 50). In contrast to genuine traveling waves (sometimes called "trigger waves"), phase waves are merely phase shifted local oscillations. They do not require lateral material transport (lateral mass redistribution) and the visual impression of

"propagation" is merely a consequence of the phase gradient. In addition to gradients, there may also be topological defects in the phase (like the spiral defect at the bottom of Fig. 1*D*, 14 µm). Continual creation and annihilation of such defects gives rise to defect-mediated turbulence (47). Finally, at large bulk heights (> 20 µm), we find traveling (spiral) waves. This is in agreement with simulations performed for the same reaction kinetics in a setup with a planar membrane on only one side of the bulk volume (39).

In summary, the model qualitatively reproduces the salient features of our experimental observations across the whole range of bulk heights remarkably well (Fig. 1*C,D*). However, the characteristic wavelength and oscillation periods of the patterns are not matched quantitatively (although they are of the same order of magnitude). Given the lack of a theoretical understanding of the principles underlying nonlinear wavelength selection, the large number of experimentally unknown reaction rates, and the potential need to further extend the model (23, 26), fitting parameters would not be informative (please refer to the *Discussion* for further elaboration on the question of length- and time-scales).

Here, we aim to reconcile *in vivo* and *in vitro* patterns on the level of the underlying pattern-forming mechanisms. We will show that several distinct mechanisms contribute to the pattern dynamics at different microchamber heights. Different characteristic types of pattern synchronization (in-phase, anti-phase, and de-synchronization) between the opposite membrane surfaces reveal the mechanisms underlying pattern formation in the experimental system. Moreover, we predict and experimentally confirm multistability of qualitatively different patterns in a regime where multiple pattern-forming mechanisms compete.

Distinct oscillation modes underlie pattern formation at different bulk heights. To identify the pattern-forming mechanisms governing the dynamics at different bulk heights, we performed a linear stability analysis of the homogeneous steady states. This analysis predicts which patterns will initially grow from small random perturbations of a homogeneous initial state. The technical details of the linear stability analysis for the reaction–diffusion model of the Min system in the microchambers' geometry (Fig. S2) are described in the *SI Materials and Methods*.

We find three types of instabilities: a lateral instability, and two types of vertical instability (membrane-to-membrane and membrane-to-bulk). As we will see in the following, the vertical instabilities correspond to vertical oscillation modes and do not require lateral redistribution of mass, and therefore are *local* instabilities. Throughout the remainder of the paper, we will use the terms local oscillation (resp. instability) and vertical oscillation (resp. instability) interchangeably.

The phase diagram in Fig. 2*A* shows the regimes where the three types of instabilities exist as a function of the bulk height and the ratio of MinE concentration and MinD concentration (short E-D ratio). Notably these regimes largely overlap, meaning that multiple distinct instabilities can be active at the same time.

Low bulk height: only lateral oscillations. At low bulk height, diffusion mixes the bulk in vertical direction quickly, such that no substantial vertical protein gradients can form (see Movie S5). Consequentially, no vertical instability can arise and the local equilibria are always locally stable (see Fig. 2*B*, top). There is, however, a lateral instability (illustrated by the green arrows in Fig. 2*B*, bottom), driven by lateral mass redistribution due to lateral cytosolic gradients which are induced by shifting stable local equilibria (51). Lateral mass redistribution also underlies the Turing instability and *in vivo* Min patterns (37). If, instead, *in vivo* Min-protein patterns were driven by local instabilities, sufficiently small cells would blink. This has never been observed experimentally. We conclude that the patterns observed *in vitro* at low bulk height are governed by the same mechanisms as those *in vivo* — a lateral mass-redistribution (Turing) instability.

Intermediate bulk height: membrane-to-membrane oscillations. At a critical bulk height H_c, a local instability sets in, corresponding to membrane-to-membrane oscillations as illustrated in Fig. 2*C*. The instability is driven by the vertical transport of proteins from one membrane to the other through the bulk (Movie S6). Characteristically, these membrane-to-membrane oscillations are in *anti-phase* between the top and the bottom membrane. This alternation in protein density will later serve as a signature of membrane-to-membrane oscillations in the experimental data. The critical height, H_c, is determined by the dynamic bulk gradients that build up as proteins that detach from one membrane are recruited to the other membrane. Its value depends on the reaction rates and bulk diffusivities. For the parameters used here, the critical bulk height, as determined by linear stability analysis, is approximately 5 µm (see Fig. 2*A*).

Notably, an analogy can be drawn to *in vivo* pole-to-pole oscillations. The two membrane "points" at the top and bottom of a local compartment in the *in vitro* system can be pictured as analogous to the cell poles *in vivo*. Hence, the vertical membrane-to-membrane oscillations *in vitro* in a laterally isolated notional compartment are equivalent to the *in vivo* pole-to-pole oscillations.

Large bulk height: membrane-to-bulk oscillations. When the bulk height is larger than the penetration depth of the bulk gradient, the bulk further away from the membranes acts as a protein reservoir and facilitates oscillations between the membrane and the bulk reservoir — individually and independently for both the top and bottom membrane, as illustrated by orange arrows in Fig. 2*D* (see also Movies S7 and S8). Diffusion from the membrane to the bulk reservoir and back provides the delay that underlies these membrane-to-bulk oscillations at a large bulk height. These oscillations are equivalent to the local oscillations in an *in vitro* setup with a membrane only at the bottom (39). The bulk reservoir in-between the membranes thus acts as a buffer that decouples the two membranes.*

Taken together, we find three different oscillation modes: one lateral mode that is driven by lateral redistribution of mass (i.e. a lateral instability) and two vertical oscillation modes that are driven by vertical exchange of proteins between the membranes and the bulk in between them. The different patterns shown in Fig. 1*D* correspond to these oscillation modes: Lateral oscillations alone drive standing waves (Movie S5). Dominance of vertical membrane-to-membrane

*Mathematically, in the linear stability analysis, the two vertical transport modes — membrane-to-membrane and membrane-to-bulk — become equivalent at large bulk heights: the vertical modes are $\sinh(z)$ and $\cosh(z)$, which asymptotically approach $\exp(z)$ for large z. Since for linear stability, only the vertical bulk-gradient at the membrane surface matters, the stability properties of these modes become identical in the asymptotic limit $H \to \infty$; see *SI Materials and Methods*.

DRAFT

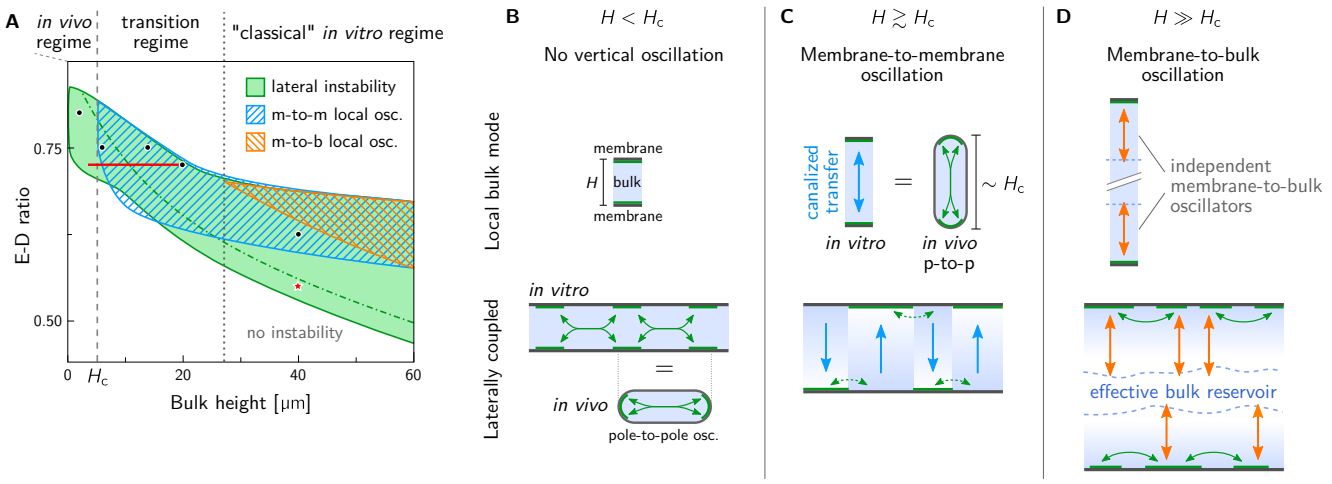

Fig. 2. Distinct lateral and local instabilities at different bulk heights. A Phase diagram for bulk height and E-D ratio showing three types of linear instabilities that exist in overlapping regimes: lateral instability (green), local membrane-to-membrane instability ("m-to-m", blue) and local membrane-to-bulk instability ("m-to-b", orange). See Fig. S3 for representative dispersion relations in the various regimes. The green dot-dashed line marks the commensurability condition for lateral instability that indicates the transition from chaotic to coherent patterns at larger bulk heights (39). A representative example of a chaotic pattern is shown in Movie S4 for the parameter combination marked by the red star. Black dots mark the parameters used for the simulations shown in Fig. 1*D*. The red line indicates the parameter range in which adiabatic sweeps of the bulk height were performed to demonstrate hysteresis as a signature of multistability (see Fig. 4 below). Panels (B–D) illustrate the instabilities at different bulk heights. The top row shows laterally isolated compartments, to illustrate local vertical oscillations due to vertical bulk gradients. The bottom row illustrates the interplay of lateral and local oscillation modes in a laterally extended system. **B** At low bulk height, where the bulk height is too small for vertical concentration gradients to form (see Movie S5). Hence, a laterally isolated compartment does not exhibit any instabilities. In a laterally extended system as depicted in the bottom row, exchange mass of mass can drive a lateral instability (green arrows). The cartoon of an *E. coli* cell illustrates that this instability also underlies pattern formation *in vivo*. **C** For bulk heights above H_c, vertical concentration gradients lead to delays in the vertical transport of proteins between top and bottom membrane (see Movie S6). Consequentially, vertical membrane-to-membrane oscillations (blue arrows) emerge that do not require lateral exchange of mass, i.e. they occur in a laterally isolated compartment. The cartoon of a *E. coli* cell illustrates that the m-to-m oscillations in vitro can also be pictured as equivalent to *in vivo* pole-to-pole oscillations, where the two cell-poles represent the top and bottom membrane of a local compartment of the in vitro system. **D** At bulk-heights larger than the penetration depth of vertical gradients, the top and bottom membrane effectively decouple (see Movies S7 and S8). In this regime, which corresponds to the classical *in vitro* regime, the bulk in-between the membranes acts as an effective protein reservoir that facilitates membrane-to-bulk oscillations.

DRAFT

oscillations leads to large-scale oscillations (Movie S6).[†] These large-scale oscillations clearly demarcate the transition from the *in-vivo*-like regime, where only lateral oscillations but no vertical oscillations exist, to the *in vitro* regime where vertical oscillations come into play. At large bulk height, the interplay of lateral oscillations and local membrane-to-bulk oscillations drives traveling waves (Movie S7) and standing wave chaos at low E-D ratios (see Movies S4 and 8 for simulations the full geometry (2+3D) and in slice geometry (1+2D), respectively). The large bulk-height regime was investigated in detail in a previous theoretical study (39). In particular, it was found that the transition from travelling waves standing wave chaos corresponds to a commensurability condition in the dispersion relation, marked by a dot-dashed green line in the phase diagram (Fig. 1*A*).

In passing, we note that the patterns we find in numerical simulations have large amplitude. It is no a priori clear whether the linear stability analysis of the homogeneous steady state is informative regarding such large amplitude patterns. In the *SI Materials and Methods*, we briefly describe how a recently developed theoretical framework called "local equilibria theory" can be used to characterize large amplitude patterns locally and regionally (39, 51). Centrally, this framework utilizes the fact that the Min-protein dynamics conserve the total amounts of MinD and MinE. Technical details and several concrete examples for local equilibria analysis of the patterns found in numerical simulations are provided in the SI and visualized in Movies S16–S18.

Interplanar pattern synchronization reveals vertical oscillation modes in experiments. Recall that the vertical synchronization of patterns on the opposite (top and bottom) membranes is a a key signature that distinguishes the lateral oscillation mode at low bulk height, the vertical membrane-to-membrane oscillation mode at intermediate bulk height, and the vertical membrane-to-bulk oscillation mode at large bulk height. Respectively, these modes correspond to strong in-phase coupling, anti-phase coupling, and de-coupuling of the dynamics on the two opposites membranes. In the following, we will use these characteristics to infer the underlying oscillation modes directly from the experimentally observed patterns.

Interplanar synchronization of patterns can be visualized by overlaying snapshots and kymographs where the protein densities on the two membranes are shown in different colors (Fig. 3*A*). Recall that at low heights, we found only lateral instability (cf. Fig. 2*B*) where the bulk is uniform in the vertical direction. This leads to strong in-phase synchronization of the top and bottom membrane (Fig. 3*B*, left). In contrast, the local instability driven by vertical membrane-to-membrane transport for leads to anti-phase synchronization (Fig. 3*B*, center; cf. Fig. 2*C*). Finally, at large height, the large bulk reservoir in between the two membranes decouples their patterns (cf. Fig. 2*D*), thus removing any synchronization between them (Fig. 3*B*, right).

To test these theoretical predictions, we imaged the Min

[†] We subsume several phenomena, including homogeneous oscillations, phase chaos, and defect-mediated turbulence (52–54), under the general term "large-scale oscillations." A detailed quantification and distinction is beyond the scope of this work. Instead, we relied on the anti-phase synchronization between top and bottom membrane that is characteristic for the membrane-to-membrane oscillation mode.

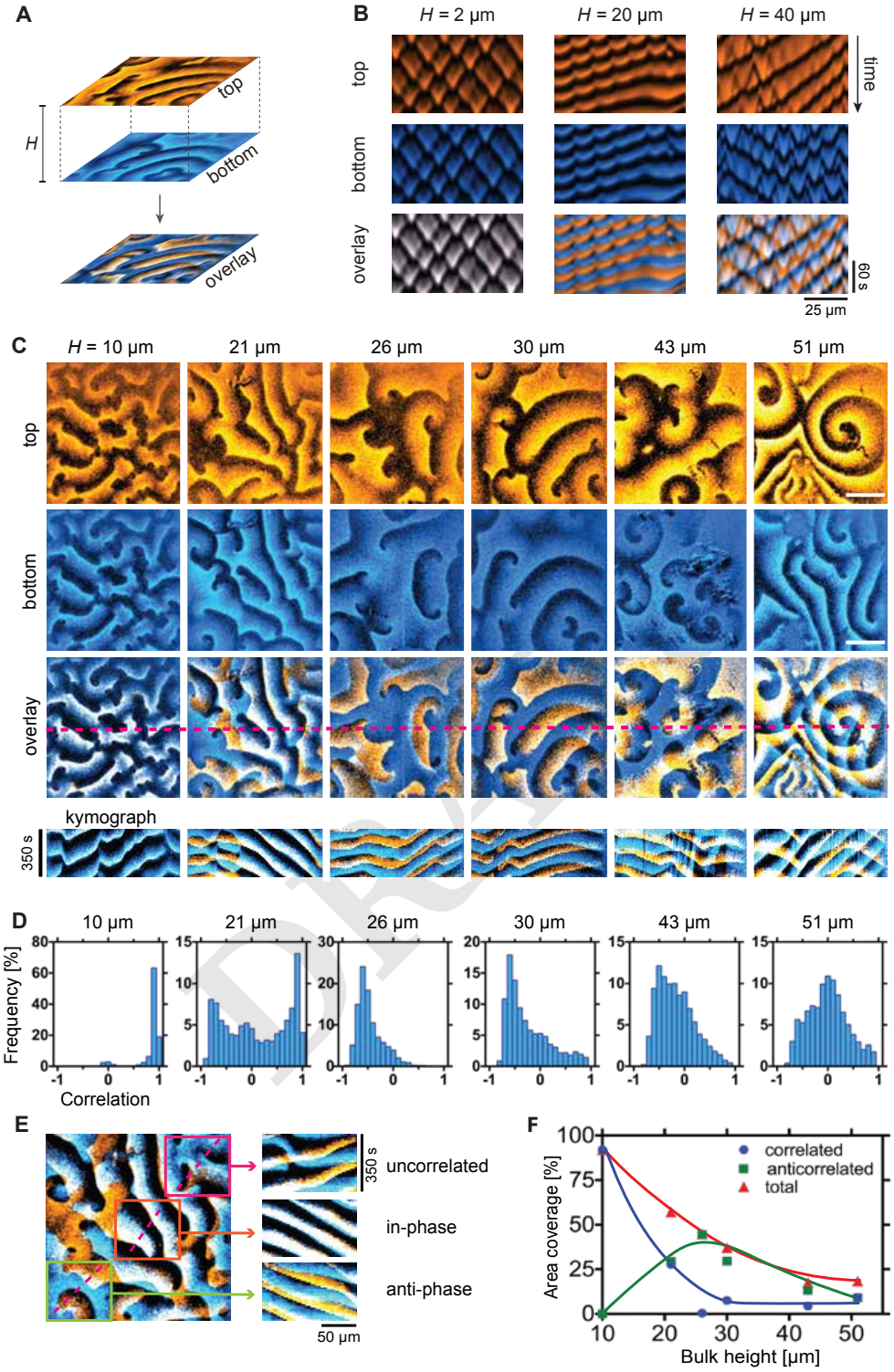

Fig. 3. Min cross-talk between opposite membranes. **A** Patterns form on the membranes both on the top and bottom surface of the microchambers. Overlaying these patterns in different colors (blue and orange) reveals the synchronization between them. **B** Kymographs from numerical simulations showing perfect in-phase synchrony of patterns at low bulk height, anti-phase synchrony driven by local membrane-to-membrane oscillations at intermediate bulk height and de-synchronization at large bulk height, where two membranes effectively decouple. (E-D ratios from left to right: 0.75, 0.725, and 0.55). **C** Snapshots and kyomographs from simulataneous (< 0.1 s delay) imaging of the top (orange) and bottom (blue) membrane in microchambers of different heights (1 µM MinD, 1 µM MinE). In the overlay, areas where peak protein concentrations coincide are white. Areas of coinciding low protein density are black. Bars correspond to 50 µm. **D** Each field of view (FOV) was divided into a grid of cells for which the correlation analysis was performed individually. Histograms show frequency distribution of correlations of individual cells in the grid measured for 30 timepoints in each FOV. Perfect in-phase correlation corresponds to a correlation value of 1 and perfect anti-phase to a value of –1 respectively; lack of correlation corresponds to a correlation measure 0. **E** Example of coexistence of in-phase and anti-phase synchrony within adjacent spatial regions. **F** Classification of top-bottom correlation as a function of bulk height, extracted from the histograms in panel D. Correlation values above 0.7 are classified as correlated, values less than –0.3 as anticorrelated.

patterns on both membranes simultaneously (delay $< 0.1\,\mathrm{s}$) in a set of experiments with bulk heights ranging from 10 to 51 µm at 1:1 E-D ratio. Figure 3*C* and Movie S9 show the patterns found in this set of experiments. In agreement with the predictions, we find fully synchronized patterns at low bulk height (10 µm). At intermediate bulk heights (21 to 30 µm) we find spatial regions where patterns are clearly synchronized in anti-phase as well as regions of in-phase synchronization. Note in particular the dominant anti-correlation at bulk heights of 26 µm and 30 µm which are a strong indication of the membrane-to-membrane oscillations predicted by the theoretical model. As the height increases further, patterns become more de-synchronized, with a near-complete dissimilarity between bottom and top at large bulk height (51 µm).

To quantify these observations, we performed a correlation analysis of the patterns on the opposite membranes (Fig. 3*D*). Because we see that spatial sub-regions within one field of view (FOV) exhibit different synchronization behavior (Fig. 3*E*), we divided each FOV into a grid of smaller sub-regions ($\approx 10 \times 10\,\mu\mathrm{m}^2$) and determined the temporal correlation between the top and bottom membrane individually for each sub-region. The averaged correlation values from all sub-regions are collected in histograms shown in Fig. 3*D*. This quantitative analysis confirms the qualitative finding from visual inspection of the snapshots and kymographs in Fig. 3*C*. At low bulk height the two membranes are almost perfectly synchronized in-phase (correlation close to 1). As the height increases, the distribution of correlation becomes bimodal as correlations close to -1 appear, indicating emerging anti-phase synchronization, which reaches its maximum at 26 µm. For larger bulk heights, the correlation measure clusters around zero, indicating de-synchronization of the patterns on the two opposite membranes.

Figure 3*F* summarizes the bulk height dependency of the pattern correlation and clearly shows that in-phase correlation is maximal at small bulk heights, anti-correlation peaks at intermediate bulk heights, and that the overall correlation decreases as bulk height increases and both membranes decouple from each other. These findings provide strong experimental evidence for the existence and importance of vertical concentration gradients in the bulk. As discussed above, the synchronization across the bulk is a consequence of the different instabilities underlying pattern formation and hence reveals the role of these instabilities in the experimental system.

Competition of multiple oscillation modes leads to multistability of patterns. In the linear stability analysis, we found that multiple types of instabilities — corresponding to distinct lateral and vertical oscillation modes — can coexist in overlapping regions of parameter space (Fig. 2*A*). In these regions, we expect multistability (and possibly coexistence) of the associated patterns as a result of the competition between multiple oscillation modes. To test this, we performed simulations where the bulk height was increased/decreased very slowly compared to the oscillation period of patterns. As a hallmark of multistability, we observed hysteresis in the transitions between the different pattern types (Fig. 4*A*–*C*). Our results from numerical simulations indicate at least threefold multistability of qualitatively different pattern types: vertically in-phase (chaotic) standing waves, vertically anti-phase homogeneous oscillations, and vertically anti-phase traveling/standing waves.

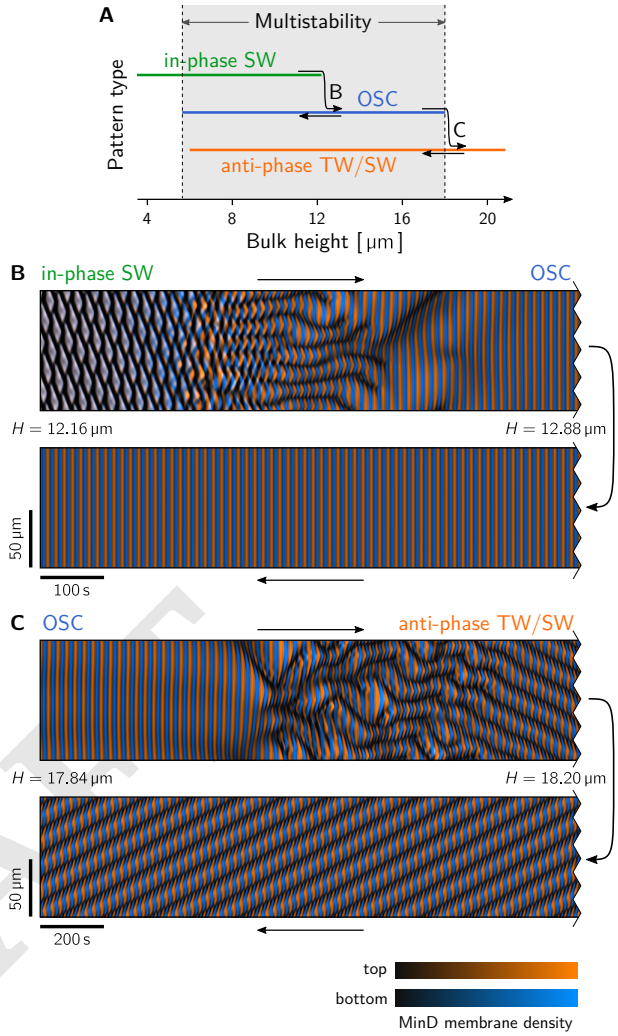

Fig. 4. Multistability and coexistence of different pattern types in numerical simulations. A Using adiabatic parameter sweeps of the bulk height (along the red line, E/D = 0.725, in Fig. 2*D*; see SI for details) we demonstrate multistability of different pattern types. A hallmark of multistability is hysteresis as shown in (B) for the transition from in-phase standing waves (SW) to homogeneous oscillations (OSC); and in (C) for the transition to homogeneous oscillations to anti-phase traveling/standing waves (TW/SW). **B** Kymograph showing the transitions from in-phase SW to anti-phase OSC as the bulk height is adiabatically increased from 12.16 µm to 12.88 µm. Upon decreasing the bulk height back to 12.16 µm, the homogeneous oscillations persist. In fact the transition back to in-phase SW takes place around $H = 6$ µm, see Fig. S7A. **C** Kymograph showing the transitions from anti-phase OSC to anti-phase TW/SW as the bulk height is adiabatically increased from 17.84 µm to 18.20 µm. Upon decreasing the bulk height back to 17.84 µm, the anti-phase TW/SW pattern persists. Similarly as OSC, these patterns persist down to around $H = 6$ µm, see Fig. S7B.

In the multistable regime, the pattern exhibited by the system depends on the initial condition (see Fig. S5). Moreover, in simulations with large system size (lateral domain size of 500 µm), we find spatiotemporal intermittency at intermediate bulk height (~ 18 µm). This phenomenon can be pictured as the coexistence of large-scale oscillations, traveling waves, and standing waves in space where they continually transitioned from one to another over time (Fig. S6A). In simulations in full 3D geometry, we observe coexistence of in-phase synchronized standing waves and large-scale anti-phase oscillations in neighboring regions regions of the membranes (Fig. S6A and

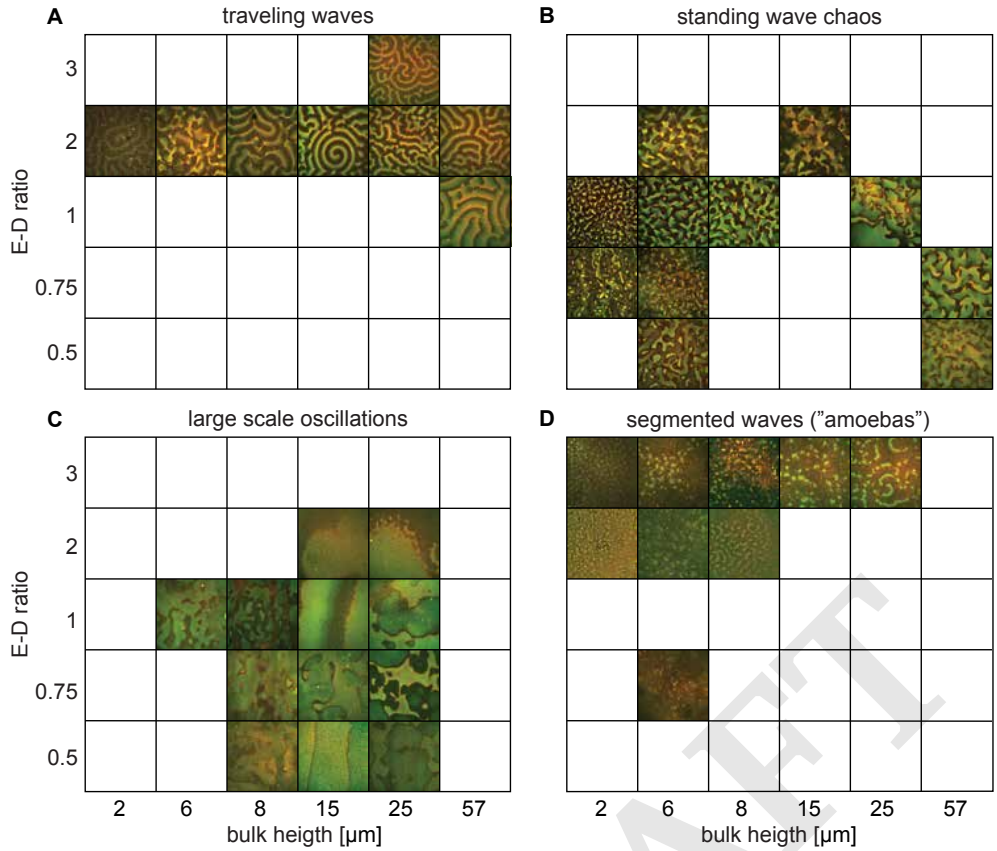

Fig. 5. Experimental phase diagram showing multistability. A–D show representative snapshots to indicate where each of the four pattern types — traveling waves (TW), standing wave chaos (SWC), large scale oscillations (OSC) and segmented waves — was observed as a function of E-D ratio and bulk height (cf. Movies S11–S14). To vary the E-D ratio, the concentration of MinE was varied from 0.5 to 3 µM at a constant MinD concentration of 1 µM. (Snapshots show overlays of MinD channel (green) and MinE channel (red); field of view: 307 µm × 307 µm.)

DRAFT

Movie S10).

To experimentally test the predicted multistability, we systematically varied the bulk height (from 2 to 57 µm) and the E-D ratio (from 0.5 to 3), and repeated the experiment several times ($N = 2$ to 5) for each parameter combination. Figure 5 and Movies 11–14 show an overview of the patterns found in this assay. Notably, at intermediate bulk heights, qualitatively different patterns were observed in repeated experiments with the same parameters, clearly indicating multistability (see the "phase diagram" in Fig. S8). This confirms our theoretical prediction from linear stability analysis and numerical simulations. For several parameter combinations ($H = 6\,\mu\text{m}, E/D = 2$ and $H = 13\,\mu\text{m}, E/D = 2$), we found threefold multistability (Movie S15).

By contrast, at low bulk height (2 µm) we found only a single instance of (twofold) multistability ($H = 2\,\mu\text{m}, E/D = 2$), whereas at large bulk height (57 µm) we did not observe any multistability at all. In agreement to these experimental findings, numerical simulations at small and large bulk heights do not show multistability of qualitatively different patterns.

Quantification of experimentally observed patterns.

Segmented waves ("amoebas"). In addition to the three pattern types presented in Figure 1, we also found a fourth type of patterns that resembles "segmented waves" (55, 56). These patterns are similar to a phenomenon previously observed in the *in vitro* Min system where it was called "amoeba pattern" (23, 28). The segmented waves consist of small separate "blobs" of MinD which, in contrast to standing waves, are not surrounded by MinE but instead feature a one-directional MinE gradient, resulting in directional propagation of the blobs (Movie S14). This type of pattern occurred mostly at large E-D ratio ($\gtrsim 1$) and for a broad range of bulk heights (2–25 µm). Due to its incoherent and non-oscillatory character, we did not characterize this pattern by autocorrelation analysis.

In the vicinity to the traveling wave regime, the segmented waves emerge due to the segmentation of the spiral wave front. Such "segmented spirals" were previously observed and studied in the BZ-AOT system (55, 56). This might provide hints towards the mechanism underlying segmented wave formation. Explaining this phenomenon likely requires an extension of the minimal Min model, e.g. by the cytosolic switching dynamics of MinE (23).

Traveling waves. As predicted by the model, traveling waves are found mainly for large bulk heights ($> 15\,\mu\text{m}$) and sufficiently large E-D ratios (≥ 1). In addition, we found in traveling waves down to 2 µm bulk height at an E-D ratio of 2. We quantified the experimentally observed patterns using autocorrelation analysis (Fig. S9). Traveling waves exhibit oscillation period that increase as a function of E-D ratio and bulk height in the range 2.5 to 8 min. Their wavelength ranged mostly from 35 to 55 µm and did not vary systematically across the conditions we investigated.

Standing wave chaos. Standing wave chaos occurs in two distinct regions of the phase diagram. First, at low bulk heights, where our theoretical analysis shows that only lateral instability exists (cf. Figs. 2 and 3). Second, we found standing wave

chaos at large bulk heights, but only at low E-D ratios, as was theoretically predicted in a previous study (39). Similarly as for the traveling waves, we found that the oscillation period of standing waves varied over a broad range (from 4 to 37 min) increasing as a function of bulk height and E-D ratio. The wavelength of standing waves is approximately 40 µm, showing a slight increase as a function of bulk height.

In addition to wavelength and oscillation frequency, we also quantified the width of fronts (also called "interfaces" or "domain walls") that connect low-density to high-density regions of the standing wave patterns (see Fig. S10). The front is around 5 µm, which is indeed quite close to the length scale of *in vivo* patterns. Because the front width is directly determined by the lateral mode underlying pattern formation (51), this provides an additional link between the *in vivo* and *in vitro* phenomena.

Large-scale oscillations (phase waves, defect-mediated turbulence). Large-scale oscillation phenomena commonly found in oscillatory media like phase waves and defect-mediated turbulence were found only at intermediate heights. They dominated at the low E-D ratios in particular, as also predicted by linear stability analysis for the mathematical model (cf. Fig. 2*A*, note the small regime around $H = 10\,\mu\text{m}$, at the lower edge of the regime of instability where only the local membrane-to-membrane oscillation mode is unstable.). We observed robust large-scale oscillations down to 8 µm bulk height and one instance at a bulk height of 6 µm, indicating the critical bulk height for the onset of membrane-to-membrane oscillations in the experiment. This value is in good agreement with the minimal model where it is about 5 µm for the parameters used in this study.

By autocorrelation analysis, we found oscillation periods between 4 min and 30 min where the period increases as a function of bulk height. As in numerical simulations, we found patterns that show the same phenomenology as defect-mediated turbulence and spatiotemporal intermittency close to the transition to the traveling (spiral) wave regime. A detailed investigation of these phenomena in the Min system is beyond the scope of this study, but an interesting direction of future research.

Conclusions

The starting point for this study was the puzzling qualitative and quantitative differences between the phenomena exhibited by the MinDE-protein system *in vivo* and *in vitro*. A principled theoretical approach together with a minimal model and direct experimental verification enabled us to disentangle the Min system's complex phenomenology and reconcile these two experimental contexts. We found that different patterns emerge from and are maintained by distinct pattern-forming mechanisms (oscillation modes) and that the key parameter controlling the transitions between these mechanisms is the bulk-surface ratio. This implies that no new biochemistry is necessary to resolve the dichotomy between *in vivo* and *in vitro* phenomenology.

The bulk height is an important control parameter for pattern formation. Our *in vitro* experiments in laterally wide, flat microchambers with a well-controlled finite height showed that the Min-protein interactions can yield dramatically different patterns by changing only the height of the confining chamber and the E-D ratio. While the important role of total densities as control parameters was shown before (both in theoretical (37, 39, 51) and experimental (23, 27) studies) our findings show that the bulk height, or more generally the bulk-surface ratio, is an equally important control parameter. Hence, controlling both the bulk-surface ratio and the enclosed total densities is essential to systematically study the Min system — a combination that was not possible to control in previous experimental setups. Importantly, our setup singles out the effect of the bulk-surface ratio, while avoiding the confounding effects of lateral geometric confinement on pattern formation (38).

Bulk-surface coupling is inherent to many pattern-forming systems beyond the Min system. Intracellular pattern formation in general is based on cycling of proteins between cytosolic and membrane/cortex-bound states; see for example the Cdc42 system in budding yeast and fission yeast (33, 57), the PAR system (45, 58) in *C. elegans*, excitable RhoA pulses in *C. elegans* (59), Xenopus and starfish oocytes (60), and MARCKS dynamics in many cell types (61, 62). Further examples include, intracellular signaling cascades (63–66) and, potentially, intercellular signaling in tissues and biofilms. Our study shows that it is essential to explicitly take the bulk-surface coupling into account when one investigates such systems.

Distinct lateral and vertical oscillation modes underlie pattern formation. In the experiments across a large range of E-D ratios and bulk heights, we found at least four qualitatively distinct pattern types: chaotic standing waves, large-scale oscillations, segmented waves patterns, and traveling waves. Clearly, a classification of the dynamics based on the topology of the protein-interaction network is not sufficient in such a situation. Instead, our theoretical analysis shows that a classification is possible in terms of the lateral and vertical oscillation modes that can be identified by linear stability analysis. While the classical linear stability analysis of a homogeneous steady state is only valid for small amplitude patterns, local equilibria theory enabled us to reveal how these instabilities drive patterns far from the homogeneous steady state. Diffusive mass redistribution between the compartments changes the equilibria and their stability properties that serve as proxies for the local dynamics. This principle made it possible to systematically identify distinct lateral and local instabilities as physical mechanisms of (strongly nonlinear) pattern formation.

On the level of pattern-forming mechanisms, we showed that the archetypical *in vivo* and *in vitro* patterns of the Min system correspond to different instabilities that arise in separate parameter regimes: lateral mass-transport oscillations at low bulk heights (*in vivo*), and two additional modes of vertical oscillations at large bulk heights (*in vitro*). Central to these distinct oscillation modes are vertical bulk gradients that couple top and bottom membrane. As a consequence of this coupling, we observed characteristic in-phase synchronization of patterns between both membranes low bulk heights and anti-phase synchronization at intermediate bulk heights. At large bulk heights, the top and bottom membrane decouple and the patterns are no longer synchronized between them. These findings serve as a clear signature of the underlying instabilities in the experimentally observed patterns. Crucially, this allowed us to characterize the observed patterns on this mechanistic level and directly link the observation to the theoretical analysis. Furthermore, synchronization of patterns

DRAFT

across the bulk serves as an experimental proof of the role of such bulk gradients for pattern formation.

A second important evidence for the distinct lateral and vertical oscillation modes are multistability and coexistence of different pattern types. Both in numerical simulations and in experiments, we found multistability in the transition regime in parameter space where multiple instabilities based on different transport modes coexist. This raises many interesting questions for future research which we will briefly discuss in the *Outlook* below.

Reconciling pattern formation *in vivo* and *in vitro*. Taken together, robust and qualitative features of the patterns — synchronization between top and bottom membrane, and multistability in the transition regime — serve as clear signatures of the underlying pattern-forming mechanisms in the experimental data. This enabled us to reconcile pattern formation *in vivo* and *in vitro* on a mechanistic level. Importantly these features are inherent to the vertical transport modes driving the pattern-forming instabilities. They can be intuitively understood (cf. Fig. 2*B*–*D*) and are not sensitive to parameter changes or model variations. This establishes a strong connection between the experimental system, the minimal model, and the theoretical framework.

Length-scale selection, pattern wavelength and front width. A major phenomenological feature of patterns that is typically discussed in the context of the *in vivo* vs *in vitro* dichotomy is the pattern wavelength. From a theoretical standpoint, however, the principles underlying nonlinear wavelength selection of large-amplitude patterns are largely unknown. As of yet, only (quasi-) stationary patterns in one- and two-variable systems have been systematically studied (67–69). Importantly, the wavelength of strongly nonlinear patterns is not necessarily determined by the dominant linear instability of the homogeneous steady state. Instead, the wavelength is subject to a subtle interplay of local reactions and lateral transport (many nonlinearly coupled modes) and therefore can depend sensibly, and non-trivially on parameters. For instance, a previous theoretical study of the *in vivo* Min system showed that a subtle interplay of recruitment, cytosolic diffusion and nucleotide exchange can give rise to "canalized transfer" which plays an important role for wavelength selection in this system (37). Moreover, experimental studies on the reconstituted Min system showed that many "microscopic" details, like the ionic strength of the aqueous medium, temperature, and membrane charge can also affect the wavelength of Min patterns (20, 22).

Matching the wavelengths found in simulations to those found in experiments would require fitting of parameters, and, potentially, model extensions (e.g. the switching of MinE (23)). Given the already large number of experimentally unknown reaction rates, such fitting would not be informative. Due to a lack of understanding of the underlying principles, fitting would also be a laborious and computationally expensive task, as one would need to "blindly" search large parameter ranges.

Besides their wavelength, i.e. the distance between consecutive wave nodes, patterns have a second characteristic length-scale — the width of fronts, also called "interfaces" or "domain walls", that connect low-density to high-density regions. While linear stability analysis of the homogeneous steady state does not predict the wavelength of large-amplitude patterns, the front width is quantitatively linked to the underlying lateral instability that creates and maintains them (51). Indeed, the front widths observed in experiments at low bulk height are of the same order of magnitude as the length scale of *in vivo* patterns ($\sim 5\,\mu\mathrm{m}$), which agrees with our finding that both are driven by the same type of (regional) lateral instability (see Fig. S10).

Understanding the principles of wavelength selection of highly nonlinear patterns in general, and the Min-protein patterns in particular, remains an open problem for future research, both theoretically and experimentally. Such an understanding might ultimately answer why the Min-pattern wavelengths are so different *in vivo* and *in vitro*.

Outlook

We found a large range of dramatically different phenomena exhibited by the *in vitro* Min system in laterally extended, vertically confined microchambers at different chamber heights and average total densities, both in experiments and in simulations. This leads to many interesting questions and connections to other pattern-forming systems. In the following, we discuss some of these promising avenues for future research.

Large-scale oscillations (lateral synchronization and defect-mediated turbulence). At intermediate heights of the microchambers, we observed a phenomenon that was not previously observed in the Min system: temporal oscillations between the opposite membranes with spatially nearly homogeneous protein concentrations (termed "large-scale oscillations"). Because each pair of opposite membrane points together with the bulk column in-between them constitutes a local oscillator, this can be understood as lateral synchronization of coupled oscillators. We found stable lateral synchronization of membrane-to-membrane oscillations at intermediate bulk heights. Towards larger bulk heights, homogeneous membrane-to-membrane oscillations become unstable, giving rise to defect-mediated turbulence, spatiotemporal intermittency, and eventually travelling wave patterns such as spirals. These phenomena are generic for oscillatory media and have been studied theoretically (see e.g. (47, 52–54) and experimentally (see e.g. (32, 48, 70, 71)). Interestingly, in contrast to membrane-to-membrane oscillations, membrane-to-bulk oscillations were never found to stably synchronize laterally, neither in experiments nor in simulations. Investigating this different behavior of the two vertical oscillation modes is an important question for future research.

More generally, synchronization of coupled oscillators is a topic of broad interest pervasive in nonlinear systems (72). Applications include catalytic surface reactions (see e.g. (70)), self-organization of motile cells (see e.g. (71)) cardiac calcium oscillations (see e.g. (73)), neural tissues (see e.g. (74)), and power grids (see e.g. (75, 76)). More specifically, for calcium oscillations in cardiac muscle tissue, the transition from laterally synchronized (i.e. homogeneous) oscillations to spirals and turbulent waves is thought to be a main reason for fibrillation (73). The molecular simplicity and experimental accessibility make the Min system a potential model system to further study oscillatory media experimentally and theoretically.

Multistability and coexistence of distinct patterns. Another intriguing phenomenon found at intermediate bulk-heights is multistability. Studying these phenomena in detail was beyond the scope of this work. What are the precise conditions under which these phenomena can be found? Can hysteresis

DRAFT

be observed in experiment, for example by employing spatial or temporal parameter ramps? In addition to multistability we found coexistence between distinct pattern types—for instance in-phase synchronized standing waves and anti-phase synchronized large scale oscillations—both in experiments and in simulations. A particular form of coexistence we have found in simulations of the Min model is spatiotemporal intermittency where regions of turbulent and ordered wave-patterns coexist and a continual interconversion form one pattern type into another takes place (54). The long observation times are required make it difficult to unambiguously identify intermittency in experiments, where observation is limited by ATP consumption and bleaching of fluorescent proteins.

Synchronization of patterns across the bulk. The different 'vertical' synchronization phenomena of patterns between the two juxtaposed membranes served as evidence for the distinct bulk modes. Going forward, such synchronization of patterns between two coupled surfaces is an interesting phenomenon in itself that deserves more detailed experimental and theoretical investigation. Previous experiments using the BZ reaction have implemented such a coupling through a membrane separating two reaction domains (77) and artificially using a camera–projector setup (78, 79). In-phase synchronization of spiral waves was found for sufficiently strong coupling. In our experiments with the Min system in flat microchambers, the coupling is inherent and we find both in-phase and anti-phase synchronization. Future theoretical work, using, for instance, a phase-reduction approach (80), might provide further insight into the principles underlying these synchronization phenomena.

Finally, coming back to the initial question what one can learn about self-organization biological systems (*in vivo*) from *in vitro* studies, our work demonstrates that varying "extrinsic" parameters such as geometry (bulk height) and protein copy numbers is a powerful approach to probe and investigate pattern-forming systems. This approach is complementary to mutation studies which can be viewed as variation of intrinsic parameters such as the protein-protein interaction network and reaction rates. In contrast to mutations, extrinsic parameters can be varied continuously on an axis. This is particularly useful to study the "phase-transitions" between different regimes. In conjunction with a systematic theoretical framework, this makes it possible to disentangle pattern-forming mechanisms. Here, the recently developed local equilibria theory served as such a theoretical framework that is able to describe both the onset and the maintenance of patterns far away from homogeneity. Going forward, we expect the Min system to remain an important experimental and theoretical model system to further develop the local equilibria theory.

Materials and Methods

Experiments were performed with purified Min proteins in PDMS microchambers and glass flow-cells coated with lipid bilayers. For details see *Experimental Materials and Methods* in the SI. The mathematical model accounting for the core set of Min-protein interactions (36, 37, 39), termed skeleton Min model, was analyzed using linear stability analysis and numerical simulations as described in the SI.

ACKNOWLEDGMENTS. We thank Laeschkir Würthner for insightful discussions and support with numerical simulations, Federico Fanalista for help with microfabrication and inspiring discussions, and Yaron Caspi for providing purified Min proteins. E.F. acknowledges support by the German Excellence Initiative via the programme 'NanoSystems Initiative Munich' (NIM) and the Deutsche Forschungsgemeinschaft (DFG) via projects B02 within the Collaborative Research Center SFB1032. F.B. acknowledges financial support by the DFG via the Research Training Group GRK2062 ('Molecular Principles of Synthetic Biology'). C.D. acknowledges support from the ERC Advanced Grant SynDiv (no. 669598) and the NanoFront and BaSyC programs.

1. E Mileykovskaya, et al., Effects of Phospholipid Composition on MinD-Membrane Interactions *in Vitro* and *in Vivo*. *J. Biol. Chem.* **278**, 22193–22198 (2003).
2. TH Szeto, SL Rowland, CL Habrukowich, GF King, The MinD Membrane Targeting Sequence Is a Transplantable Lipid-binding Helix. *J. Biol. Chem.* **278**, 40050–40056 (2003).
3. M Loose, K Kruse, P Schwille, Protein Self-Organization: Lessons from the Min System. *Annu. Rev. Biophys.* **40**, 315–336 (2011).
4. KT Park, et al., The Min Oscillator Uses MinD-Dependent Conformational Changes in MinE to Spatially Regulate Cytokinesis. *Cell* **146**, 396–407 (2011).
5. LD Renner, DB Weibel, MinD and MinE Interact with Anionic Phospholipids and Regulate Division Plane Formation in *Escherichia coli*. *J. Biol. Chem.* **287**, 38835–38844 (2012).
6. S Du, J Lutkenhaus, MipZ: One for the Pole, Two for the DNA. *Mol. Cell* **46**, 239–240 (2012).
7. M Zheng, et al., Self-Assembly of MinE on the Membrane Underlies Formation of the MinE Ring to Sustain Function of the *Escherichia coli* Min System. *J. Biol. Chem.* **289**, 21252–21266 (2014).
8. DM Raskin, PAJ de Boer, Rapid pole-to-pole oscillation of a protein required for directing division to the middle of Escherichia coli. *Proc. Natl. Acad. Sci.* **96**, 4971–4976 (1999).
9. F Wu, BGC van Schie, JE Keymer, C Dekker, Symmetry and scale orient Min protein patterns in shaped bacterial sculptures. *Nat. Nanotechnol.* **10**, 719–726 (2015).
10. Z Hu, J Lutkenhaus, A conserved sequence at the C-terminus of MinD is required for binding to the membrane and targeting MinC to the septum: Role of C-terminus of MinD. *Mol. Microbiol.* **47**, 345–355 (2003).
11. Z Hu, J Lutkenhaus, Topological regulation of cell division in Escherichia coli involves rapid pole to pole oscillation of the division inhibitor MinC under the control of MinD and MinE. *Mol. Microbiol.* **34**, 82–90 (1999).
12. SC Cordell, Crystal structure of the bacterial cell division inhibitor MinC. *The EMBO J.* **20**, 2454–2461 (2001).
13. A Dajkovic, G Lan, SX Sun, D Wirtz, J Lutkenhaus, MinC Spatially Controls Bacterial Cytokinesis by Antagonizing the Scaffolding Function of FtsZ. *Curr. Biol.* **18**, 235–244 (2008).
14. HI Adler, WD Fisher, A Cohen, AA Hardigree, Miniature Escherichia coli cells Deficient in DNA. *Proc. Natl. Acad. Sci.* **57**, 321–326 (1967).
15. PA de Boer, RE Crossley, LI Rothfield, A division inhibitor and a topological specificity factor coded for by the minicell locus determine proper placement of the division septum in E. coli. *Cell* **56**, 641–649 (1989).
16. M Loose, E Fischer-Friedrich, J Ries, K Kruse, P Schwille, Spatial Regulators for Bacterial Cell Division Self-Organize into Surface Waves in Vitro. *Science* **320**, 789–792 (2008).
17. V Ivanov, K Mizuuchi, Multiple modes of interconverting dynamic pattern formation by bacterial cell division proteins. *Proc. Natl. Acad. Sci.* **107**, 8071–8078 (2010).
18. K Zieske, P Schwille, Reconstitution of Pole-to-Pole Oscillations of Min Proteins in Microengineered Polydimethylsiloxane Compartments. *Angewandte Chemie Int. Ed.* **52**, 459–462 (2013).
19. K Zieske, P Schwille, Reconstitution of self-organizing protein gradients as spatial cues in cell-free systems. *eLife* **3**, e03949 (2014).
20. AG Vecchiarelli, M Li, M Mizuuchi, K Mizuuchi, Differential affinities of MinD and MinE to anionic phospholipid influence Min patterning dynamics *in vitro*: Flow and lipid composition effects on Min patterning. *Mol. Microbiol.* **93**, 453–463 (2014).
21. K Zieske, G Chwastek, P Schwille, Protein Patterns and Oscillations on Lipid Monolayers and in Microdroplets. *Angewandte Chemie Int. Ed.* **55**, 13455–13459 (2016).
22. Y Caspi, C Dekker, Mapping out Min protein patterns in fully confined fluidic chambers. *eLife* **5**, e19271 (2016).
23. J Denk, et al., MinE conformational switching confers robustness on self-organized Min protein patterns. *Proc. Natl. Acad. Sci.* **115**, 4553–4558 (2018).
24. S Kohyama, N Yoshinaga, M Yanagisawa, K Fujiwara, N Doi, Cell-sized confinement controls generation and stability of a protein wave for spatiotemporal regulation in cells. *eLife* **8**, e44591 (2019).
25. E Godino, et al., De novo synthesized Min proteins drive oscillatory liposome deformation and regulate FtsA-FtsZ cytoskeletal patterns. *Nat. Commun.* **10** (2019).
26. P Glock, F Brauns, J Halatek, E Frey, P Schwille, Design of biochemical pattern forming systems from minimal motifs. *eLife* **8**, e48646 (2019).
27. P Glock, et al., Stationary Patterns in a Two-Protein Reaction-Diffusion System. *ACS Synth. Biol.* **8**, 148–157 (2019).
28. AG Vecchiarelli, et al., Membrane-bound MinDE complex acts as a toggle switch that drives Min oscillation coupled to cytoplasmic depletion of MinD. *Proc. Natl. Acad. Sci.* **113**, E1479–E1488 (2016).
29. BP Belousov, Periodically acting reaction and its mechanism. *Collect. Short Pap. on Radiat. Medicine*, 145 (1959).
30. AM Zhabotinsky, Periodical oxidation of malonic acid in solution (a study of the Belousov reaction kinetics). *Biofizika*, 306–311 (1964).
31. RJ Field, M Burger, eds., *Oscillations and Traveling Waves in Chemical Systems*. (Wiley, New York), (1985).
32. IR Epstein, Coupled chemical oscillators and emergent system properties. *Chem. Commun.* **50**, 10758–10767 (2014).
33. E Bi, HO Park, Cell Polarization and Cytokinesis in Budding Yeast. *Genetics* **191**, 347–387

DRAFT

(2012).
34. M Howard, AD Rutenberg, S de Vet, Dynamic Compartmentalization of Bacteria: Accurate Division in *E. Coli*. *Phys. Rev. Lett.* **87** (2001).
35. K Kruse, A Dynamic Model for Determining the Middle of Escherichia coli. *Biophys. J.* **82**, 618–627 (2002).
36. KC Huang, Y Meir, NS Wingreen, Dynamic structures in Escherichia coli: Spontaneous formation of MinE rings and MinD polar zones. *Proc. Natl. Acad. Sci.* **100**, 12724–12728 (2003).
37. J Halatek, E Frey, Highly Canalized MinD Transfer and MinE Sequestration Explain the Origin of Robust MinCDE-Protein Dynamics. *Cell Reports* **1**, 741–752 (2012).
38. F Wu, et al., Multistability and dynamic transitions of intracellular Min protein patterns. *Mol. Syst. Biol.* **12**, 873 (2016).
39. J Halatek, E Frey, Rethinking pattern formation in reaction–diffusion systems. *Nat. Phys.* **14**, 507 (2018).
40. AM Turing, The chemical basis of morphogenesis. *Philos. Transactions Royal Soc. London. Ser. B, Biol. Sci.* **237**, 37–72 (1952).
41. AS Mikhailov, *Foundations of Synergetics I: Distributed Active Systems*. (Springer Berlin Heidelberg, Berlin, Heidelberg), (1990) OCLC: 851371203.
42. P Ashwin, S Coombes, R Nicks, Mathematical Frameworks for Oscillatory Network Dynamics in Neuroscience. *The J. Math. Neurosci.* **6** (2016).
43. T Litschel, B Ramm, R Maas, M Heymann, P Schwille, Beating Vesicles: Encapsulated Protein Oscillations Cause Dynamic Membrane Deformations. *Angewandte Chemie Int. Ed.* **57**, 16286–16290 (2018).
44. D Thalmeier, J Halatek, E Frey, Geometry-induced protein pattern formation. *Proc. Natl. Acad. Sci.* **113**, 548–553 (2016).
45. R Geßele, J Halatek, L Würthner, E Frey, Geometric cues stabilise long-axis polarisation of PAR protein patterns in C. elegans. *bioRxiv* (2019).
46. YL Shih, et al., Active Transport of Membrane Components by Self-Organization of the Min Proteins. *Biophys. J.* **116**, 1469–1482 (2019).
47. P Coullet, L Gil, J Lega, Defect-mediated turbulence. *Phys. Rev. Lett.* **62**, 1619–1622 (1989).
48. Q Ouyang, JM Flesselles, Transition from spirals to defect turbulence driven by a convective instability. *Nature* **379**, 143–146 (1996).
49. G Bordiougov, H Engel, From trigger to phase waves and back again. *Phys. D: Nonlinear Phenom.* **215**, 25–37 (2006).
50. EJ Reusser, RJ Field, The transition from phase waves to trigger waves in a model of the Zhabotinskii reaction. *J. Am. Chem. Soc.* **101**, 1063–1071 (1979).
51. F Brauns, J Halatek, E Frey, Phase-space geometry of reaction–diffusion dynamics. *arXiv:1812.08684 [nlin, physics:physics]* (2018).
52. MC Cross, PC Hohenberg, Pattern formation outside of equilibrium. *Rev. Mod. Phys.* **65**, 851–1112 (1993).
53. MC Cross, PC Hohenberg, Spatiotemporal Chaos. *Science* **263**, 1569–1570 (1994).
54. H Chate, Spatiotemporal intermittency regimes of the one-dimensional complex Ginzburg-Landau equation. *Nonlinearity* **7**, 185–204 (1994).
55. VK Vanag, IR Epstein, Segmented spiral waves in a reaction-diffusion system. *Proc. Natl. Acad. Sci.* **100**, 14635–14638 (2003).
56. IR Epstein, JA Pojman, *An Introduction to Nonlinear Chemical Dynamics: Oscillations, Waves, Patterns, and Chaos*, Topics in Physical Chemistry. (Oxford University Press, New York), (1998).
57. Jg Chiou, MK Balasubramanian, DJ Lew, Cell Polarity in Yeast. *Annu. Rev. Cell Dev. Biol.* **33**, 77–101 (2017).
58. NW Goehring, et al., Polarization of PAR Proteins by Advective Triggering of a Pattern-Forming System. *Science* **334**, 1137–1141 (2011).
59. JB Michaux, FB Robin, WM McFadden, EM Munro, Excitable RhoA dynamics drive pulsed contractions in the early *C. elegans* embryo. *The J. Cell Biol.* **217**, 4230–4252 (2018).
60. WM Bement, et al., Activator–inhibitor coupling between Rho signalling and actin assembly makes the cell cortex an excitable medium. *Nat. Cell Biol.* **17**, 1471–1483 (2015).
61. M El Amri, U Fitzgerald, G Schlosser, MARCKS and MARCKS-like proteins in development and regeneration. *J. Biomed. Sci.* **25** (2018).
62. S Alonso, M Bär, Modeling domain formation of MARCKS and protein kinase C at cellular membranes. *EPJ Nonlinear Biomed. Phys.* **2**, 1 (2014).
63. BN Kholodenko, Cell-signalling dynamics in time and space. *Nat. Rev. Mol. Cell Biol.* **7**, 165–176 (2006).
64. W Giese, G Milicic, A Schröder, E Klipp, Spatial modeling of the membrane-cytosolic interface in protein kinase signal transduction. *PLOS Comput. Biol.* **14**, e1006075 (2018).
65. A Cugno, TM Bartol, TJ Sejnowski, R Iyengar, P Rangamani, Geometric principles of second messenger dynamics in dendritic spines. *Sci. Reports* **9** (2019).
66. M Bell, T Bartol, T Sejnowski, P Rangamani, Dendritic spine geometry and spine apparatus organization govern the spatiotemporal dynamics of calcium. *The J. Gen. Physiol.* **151**, 1017–1034 (2019).
67. P Politi, C Misbah, When Does Coarsening Occur in the Dynamics of One-Dimensional Fronts? *Phys. Rev. Lett.* **92** (2004).
68. T Kolokolnikov, T Erneux, J Wei, Mesa-type patterns in the one-dimensional Brusselator and their stability. *Phys. D: Nonlinear Phenom.* **214**, 63–77 (2006).
69. T Kolokolnikov, M Ward, J Wei, Self-replication of mesa patterns in reaction–diffusion systems. *Phys. D: Nonlinear Phenom.* **236**, 104–122 (2007).
70. S Jakubith, HH Rotermund, W Engel, A von Oertzen, G Ertl, Spatiotemporal concentration patterns in a surface reaction: Propagating and standing waves, rotating spirals, and turbulence. *Phys. Rev. Lett.* **65**, 3013–3016 (1990).
71. S Sawai, PA Thomason, EC Cox, An autoregulatory circuit for long-range self-organization in Dictyostelium cell populations. *Nature* **433**, 323–326 (2005).
72. S Strogatz, *Sync: The Emerging Science of Spantaneous Order.* (Penguin Books, London), (2004) OCLC: 984745516.
73. AT Winfree, *When Time Breaks down: The Three-Dimensional Dynamics of Electrochemical Waves and Cardiac Arrhythmias.* (Princeton University Press, Princeton, N.J), (1987).
74. F Varela, JP Lachaux, E Rodriguez, J Martinerie, The brainweb: Phase synchronization and large-scale integration. *Nat. Rev. Neurosci.* **2**, 229–239 (2001).
75. AE Motter, SA Myers, M Anghel, T Nishikawa, Spontaneous synchrony in power-grid networks. *Nat. Phys.* **9**, 191–197 (2013).
76. M Rohden, A Sorge, M Timme, D Witthaut, Self-Organized Synchronization in Decentralized Power Grids. *Phys. Rev. Lett.* **109** (2012).
77. D Winston, M Arora, J Maselko, V Gáspár, K Showalter, Cross-membrane coupling of chemical spatiotemporal patterns. *Nature* **351**, 132–135 (1991).
78. M Hildebrand, J Cui, E Mihaliuk, J Wang, K Showalter, Synchronization of spatiotemporal patterns in locally coupled excitable media. *Phys. Rev. E* **68**, 026205 (2003).
79. S Weiss, RD Deegan, Weakly and strongly coupled Belousov-Zhabotinsky patterns. *Phys. Rev. E* **95**, 022215 (2017).
80. H Nakao, T Yanagita, Y Kawamura, Phase-Reduction Approach to Synchronization of Spatiotemporal Rhythms in Reaction-Diffusion Systems. *Phys. Rev. X* **4**, 021032 (2014).

DRAFT